

### **OPEN ACCESS**

EDITED BY Ashish Diwan, University of New South Wales, Australia

REVIEWED BY
Ying Shen,
The First Affiliated Hospital of Nanjing Medical
University, China
Peter Herman,
Yale University, United States

\*CORRESPONDENCE
Xiaopei Sun

☑ sarapennysun@yeah.net
Jun-Peng Zhang
☑ zhangjunpeng@shutcm.edu.cn
Yuehuan Zheng
☑ flinggaga@163.com

<sup>†</sup>These authors have contributed equally to this work

RECEIVED 01 March 2025 ACCEPTED 03 November 2025 PUBLISHED 20 November 2025

### CITATION

Zhang J, Wang N, Ren L-M, Sun X, Zhang J-P and Zheng Y (2025) Application of functional magnetic resonance imaging in identifying responsible brain regions associated with spinal diseases related pain. *Front. Med.* 12:1585799. doi: 10.3389/fmed.2025.1585799

## COPYRIGHT

© 2025 Zhang, Wang, Ren, Sun, Zhang and Zheng. This is an open-access article distributed under the terms of the Creative Commons Attribution License (CC BY). The use, distribution or reproduction in other forums is permitted, provided the original author(s) and the copyright owner(s) are credited and that the original publication in this journal is cited, in accordance with accepted academic practice. No use, distribution or reproduction is permitted which does not comply with these terms.

# Application of functional magnetic resonance imaging in identifying responsible brain regions associated with spinal diseases related pain

Jing Zhang<sup>1†</sup>, Nannan Wang<sup>2†</sup>, Le-Meng Ren<sup>3†</sup>, Xiaopei Sun<sup>©3,4</sup>\*, Jun-Peng Zhang<sup>©5</sup>\* and Yuehuan Zheng<sup>©3</sup>\*

<sup>1</sup>Department of Radiology, Ruijin Hospital, Shanghai Jiao Tong University School of Medicine, Shanghai, China, <sup>2</sup>Department of Nursing, Ruijin Hospital, Shanghai Jiao Tong University School of Medicine, Shanghai, China, <sup>3</sup>Department of Orthopaedics, Ruijin Hospital, Shanghai Jiao Tong University School of Medicine, Shanghai, China, <sup>4</sup>Department of Rehabilitation, Shanghai Ruijin Rehabilitation Hospital, Shanghai, China, <sup>5</sup>School of Rehabilitation Science, Shanghai University of Traditional Chinese Medicine, Shanghai, China

**Background:** Spinal diseases related pain represents a critical clinical issue that demands urgent resolution. Current treatment and assessment strategies predominantly focus on peripheral mechanisms. The application of functional magnetic resonance imaging (fMRI) offers a promising approach to identifying potential central targets for intervention.

**Methods:** We retrospectively included 31 patients with spinal diseases related pain and 32 controls with non-spinal, orthopedic complaints (no chronic neurological or psychiatric disorders). All participants underwent resting-state brain fMRI (eyes closed, awake). We quantified amplitude of low-frequency fluctuations (ALFF) with mean normalization (mALFF) and z-transformation (zALFF), regional homogeneity (ReHo; 27-voxel neighborhood), seed-based functional connectivity (FC; pre/postcentral seeds), and degree centrality (DC; binary and weighted). Between group tests used voxel-wise two-sample t\_tests with Gaussian random field (GRF) correction.

**Results:** Patient group was associated with increased m/zALFF in right cerebellar lobule IX and right Superior Frontal Gyrus, medial part, and lower activity in bilateral postcentral gyri and the cuneus, decreased m/zALFF in bilateral postcentral gyri. ReHo analysis confirmed reduced local synchrony in postcentral regions, spatially overlapping with ALFF findings. FC analyses revealed enhanced cerebellar-thalamic connectivity (Crus1/2, thalamus) but reduced connectivity in sensorimotor and higher-order cortical networks. DC showed hyperconnectivity in left cerebellar Crus I with reduced Superior Frontal Orbital (Frontal\_Sup\_Orb). All findings survived GRF correction at the pre\_specified thresholds.

**Conclusion:** Resting-state brain fMRI indicates a cerebello-thalamo-cortical alteration pattern in spinal diseases related pain featuring cerebellar involvement, prefrontal subspecialization, and multilevel sensorimotor disruption. These cross-sectional associations may inform hypothesis-generation for future neuromodulation studies and provide candidate biomarkers for monitoring, pending prospective validation.

KEYWORDS

brain map, spinal diseases related pain, responsible brain region, functional magnetic resonance imaging, brain remodeling

# 1 Introduction

Spinal diseases related pain is a leading cause of disability and health-care expenditure worldwide (1, 2). Importantly, the term "spinal diseases" refers to clinically defined conditions (e.g., disc degeneration, spinal stenosis, spondylosis), whereas commonly cited lifetime prevalence figures (e.g., for non-specific low back pain) describe a symptom rather than a diagnosis (3, 4). To avoid conflation, here we focus on patients with symtoms of spinal diseases related pain.

Spinal diseases related pain is traditionally managed through peripheral interventions such as pharmacotherapy (5, 6), physical therapy (7), or surgery (8, 9), etc. However, these approaches often fail to address central nervous system alterations increasingly recognized in chronic pain states (10–12). Resting-state fMRI has emerged as a valuable tool to identify central biomarkers, including ALFF (13–17), ReHo (15, 17, 18), and functional connectivity (10, 11, 19, 20). Recent studies have reported brain network changes (21–26), particularly in sensorimotor, limbic, and thalamo-cortical circuits, highlighting the need for a shift toward centrally focused models of spinal pain pathophysiology.

This study used fMRI to investigate the brain remodeling mechanisms of spinal diseases related pain and to identify the specific brain mapping patterns involved in pain processing pathways. The primary objective was to establish a comprehensive evaluation framework for assessing responsible brain region and connection alterations in patients with spinal diseases related pain. By implementing a central-peripheral integrated assessment system, this research aims to provide a robust scientific foundation for enhancing diagnostic accuracy, optimizing therapeutic interventions, and improving prognostic evaluation in the management of spinal diseases related pain (5–9, 27, 28).

# 2 Methods

# 2.1 Study design and participants

This retrospective study enrolled participants who underwent functional magnetic resonance imaging (fMRI) examinations at the Department of Orthopedics, Ruijin Hospital, Shanghai Jiao Tong University School of Medicine, between October 2023 and October 2024. The study protocol was approved by the Institutional Review Board of Ruijin Hospital (Ethical Approval Number: 20240902113233506). This retrospective study included two groups: (i) patients with symptoms of spinal diseases related pain due to clinically diagnosed spinal pathology (e.g., disc degeneration, osteoporotic fracture, stenosis), and (ii) controls who presented with non-spinal orthopedic complaints and no history of chronic neurological or psychiatric disorders. All participants were right-handed and underwent brain fMRI on the same 3.0-T scanner within the same institutional protocol. Major

exclusion criteria for both groups were prior spinal surgery, major neurological disease (e.g., stroke, traumatic brain injury, neurodegeneration), major psychiatric illness, claustrophobia, unstable systemic disease, or incomplete records. Pain intensity (VAS) was extracted from clinical records closest to the scan date.

# 2.2 fMRI acquisition

All data were acquired on a GE 3.0-T system. Participants lay supine, eyes closed, relaxed but awake. Resting-state functional images used gradient-echo EPI with the following parameters: TR/ TE = 2000/30 ms, flip angle = 90°, 43 axial slices, interleaved order, slice thickness = 3.2 mm (voxel  $3.4 \times 3.4 \times 3.2$  mm³), matrix  $64 \times 64$ , FOV  $220 \times 220$  mm², 240 volumes, parallel acceleration = 2. Anatomical T1-weighted images used a 3D SPGR sequence: TR/ TE = 8100/3.1 ms, flip angle =  $8^\circ$ , 176 sagittal slices, isotropic 1 mm³ voxels, FOV  $256 \times 256$  mm². The first 10 rs-fMRI volumes were discarded to allow signal stabilization.

# 2.3 Preprocessing and first-level metrics

Preprocessing was performed in RESTplus (29)(SPM12-based) on MATLAB R2013b. Steps included slice-timing correction; rigid-body realignment (subjects with >3 mm translation or >3° rotation were excluded); normalization to MNI152 template; and nuisance regression (24-parameter motion, white matter, CSF). Data were band-pass filtered at 0.01–0.08 Hz. ALFF was computed and expressed as mean-normalized (mALFF) and z-standardized (zALFF) maps within a gray matter mask (30). ReHo (31) was computed using Kendall's coefficient over a 27-voxel (3  $\times$  3  $\times$  3) neighborhood and then spatially smoothed with a 6 mm FWHM Gaussian kernel.

T1-weighted structural MRI provided the anatomical reference for EPI-anatomical registration, MNI normalization, tissue segmentation (GM/WM/CSF) for nuisance modeling, and ROI/surface definitions.

# 2.4 Functional connectivity and degree centrality

Seed-based functional connectivity (FC) analyses used bilateral precentral and postcentral gyri as *a priori* regions of interest due to their established roles in pain-related sensorimotor processing and representations of nociceptive input. Seed time series were correlated with whole-brain voxels and Fisher-z transformed. Degree centrality (DC) was computed in both binary and weighted forms using RESTplus defaults (voxelwise correlation matrix thresholding), providing complementary indices of network hubness. Exact parameter settings are reported to facilitate replication.

# 2.5 Group-level statistics

Between group comparisons employed voxel-wise two-sample  $t_{\rm L}$ tests in SPM 12(32, 33)with age and sex as covariates. Multiple comparisons were controlled with Gaussian Random Field (GRF) correction at the pre-specified thresholds (ALFF/ReHo/FC: voxel p < 0.01, cluster p < 0.01; DC: voxel p < 0.05, cluster p < 0.05, matching the original analysis). Clinical variables were summarized as mean  $\pm$  SD and compared with t-tests or  $\chi^2$  tests as appropriate (two-tailed p < 0.05) by SPSS (version 26.0; IBM, Armonk, NY, United States) statistical software.

# 3 Results

# 3.1 Participant characteristics

Thirty-one spinal diseases related pain patients (15 males/16 females;  $64.52 \pm 16.40$  years) and 32 controls (9 males/23 females;  $47.69 \pm 13.45$  years) were included after quality control. Groups did not differ in sex distribution (p > 0.05); VAS pain scores were higher in patient group (p < 0.001). Age was included as a covariate in imaging analyses. The demographic and clinical characteristics of patients are shown in Table 1.

3.2 The regional brain change in patient group

Regional spontaneous activity (mALFF / zALFF) (Tables 2, 3; Figures 1, 2): Relative to controls, patients showed higher mALFF in the right cerebellar lobule IX (MNI -6, -39, -57; cluster = 276; t = 4.8383) and right medial superior frontal gyrus (MNI – 21, 12, 33; cluster = 465; t = 4.2789). Lower mALFF emerged in the bilateral postcentral gyrus [left: MNI -57, -12, 30; cluster =501; t = -5.3963; right: MNI 48, -21, 36; cluster = 695; t = -4.957], right cuneus (MNI 0, -84, 27; cluster = 443; t = -4.5173), and right middle temporal gyrus (MNI 57, -57, 6; cluster = 77; t = -3.8437). The zALFF map reproduced this pattern: increased activity in right cerebellar lobule IX (MNI - 6, -39, -57; cluster = 310; t = 4.8195) and right medial superior frontal gyrus (MNI - 6, 39, 54; cluster = 405; t = 4.1027), and decreased activity in the bilateral postcentral gyrus [left: MNI - 57, -12, 30; cluster = 534; t = -5.6379; right: MNI 42, -18, 54; cluster = 730; t = -5.1794] and right cuneus (MNI 0, -84, 27; cluster = 443; t = -4.7479).

Regional homogeneity (ReHo) (Table 4; Figure 3): Using the SMKCC method, ReHo decreased in the left postcentral gyrus (MNI -57, -12, 27; cluster =641; t=-5.2072) and right postcentral gyrus (MNI 27, -21, 75; cluster =680; t=-5.5139).

TABLE 1 Participant characteristics.

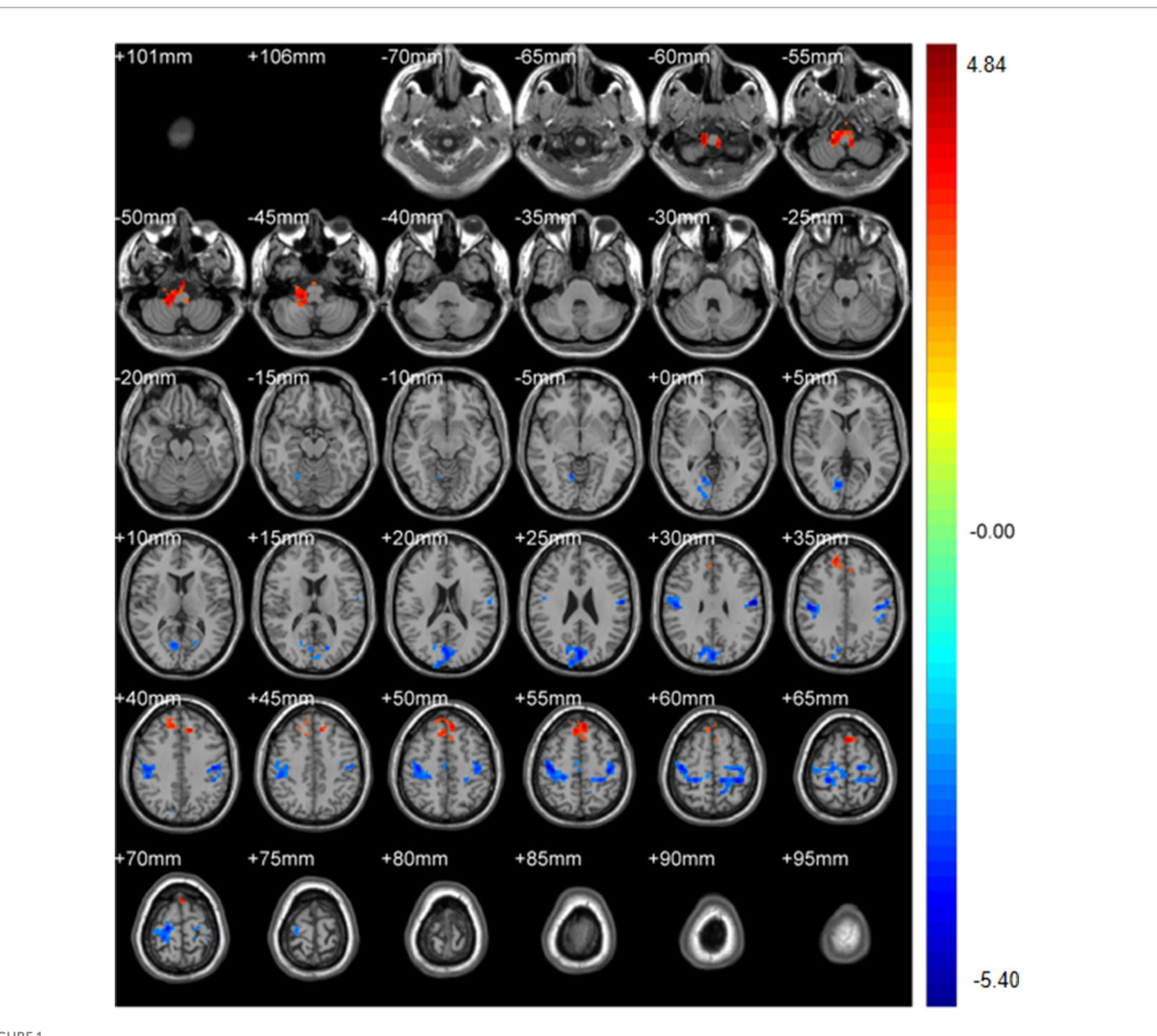
Variables	Patients (n = 31)	Controls (n = 33)	p value
Age(y)	64.52 ± 16.40	47.69 ± 13.45	<0.001
Men (n, %)	15(48.4)	9 (27.3)	0.081
VAS score	5.26 ± 1.90	1.06 ± 2.58	<0.001

TABLE 2 mALFF differences.

Brain regions	Hemisphere	Cluster size	r size Cluster centroid MNI Coordinates			t-value
			Х	Υ	Z	
Cerebellum_9	R	276	-6	-39	-57	4.8383
Cuneus	R	443	0	-84	27	-4.5173
Temporal_Mid	R	77	57	-57	6	-3.8437
Postcentral	L	501	-57	-12	30	-5.3963
Postcentral	R	695	48	-21	36	-4.957
Frontal_Sup_Medial	R	465	-21	12	33	4.2789

TABLE 3 zALFF differences.

Brain regions	Hemisphere	Cluster size	Cluster ce	oordinates	t-value	
			Х	Υ	Z	
Cerebellum_9	R	310	-6	-39	-57	4.8195
Cuneus	R	443	0	-84	27	-4.7479
Postcentral	L	534	-57	-12	30	-5.6379
Postcentral	R	730	42	-18	54	-5.1794
Frontal_Sup_Medial	R	405	-6	39	54	4.1027



mALFF analysis. Two-sample t-test results are presented. Areas in red indicate significantly increased mALFF value. Areas in blue indicate significantly decreased mALFF value. In the comparison of mALFF value between patient group compared to control group showed significantly increased mALFF in Cerebellum\_9\_R and right Frontal\_Sup\_Medial\_R.

# 3.3 The whole brain changes in patient group

Seed-based functional connectivity (FC) (Tables 5–8; Figures 4–7):

Postcentral gyrus seeds: Left postcentral seed: showed stronger FC with left cerebellar Crus I (MNI -42, -63, -36; cluster = 131; t=4.4727) and left thalamus (MNI -18, -21, 12; cluster = 67; t=4.1848); showed weaker FC with right precentral gyrus (MNI 39, -15, 51; cluster = 104; t=-4.1961), left postcentral gyrus (MNI -27, -33, 66; cluster = 113; t=-4.1962), and right paracentral lobule (MNI 9, -21, 69; cluster = 160; t=-4.3763). Right postcentral seed: showed stronger FC with left cerebellar Crus II (MNI -30, -57, -45; cluster = 129; t=4.4861) and right cerebellar Crus I (MNI 15, -51, -45; cluster = 127; t=4.6384); showed weaker FC with left superior temporal gyrus (MNI -54, -12, 27; cluster = 197; t=-5.1077), right calcarine cortex (MNI 12, -51, 0; cluster = 76; t=-3.9785), right precentral gyrus (MNI 39,

-15, 54; cluster = 316; t = -5.2055), and left postcentral gyrus (MNI -45, -15, 54; cluster = 137; t = -4.4583).

Precentral gyrus seeds: Left precentral seed: showed stronger FC with left cerebellar Crus II (MNI -42, 60, -39; cluster = 198; t = 4.495) and with the thalamus bilaterally [right thalamus (MNI 15, -15, 12; cluster = 58; t = 4.5659) and left thalamus (MNI -15, -21, 12; cluster = 55; t = 4.9435)]; showed weaker FC with left superior temporal gyrus (MNI – 45, 18, 12; cluster = 115; t = -4.5627), left cuneus (MNI – 9, –84, 24; cluster = 63; t = -4.0804), left postcentral gyrus (MNI – 39, –27, 57; cluster = 321; t = -4.7458), right postcentral gyrus (MNI 36, -36, 60; cluster = 143; t = -4.6398), and right superior frontal gyrus (MNI 27, -24, 75; cluster = 108; t = -4.233). Right precentral seed: showed stronger FC with right cerebellar Crus I (MNI 30, -75, -36; cluster = 235; t = 5.0247) and left cerebellar Crus II (MNI – 3, –69, –30; cluster = 214; t = 4.685); showed weaker FC with right superior temporal gyrus (MNI – 45, -18, 12; cluster = 200; t = -5.1304), left postcentral gyrus (MNI -42, -18, 51; cluster = 186; t = -4.0706), right postcentral gyrus (MNI 42,

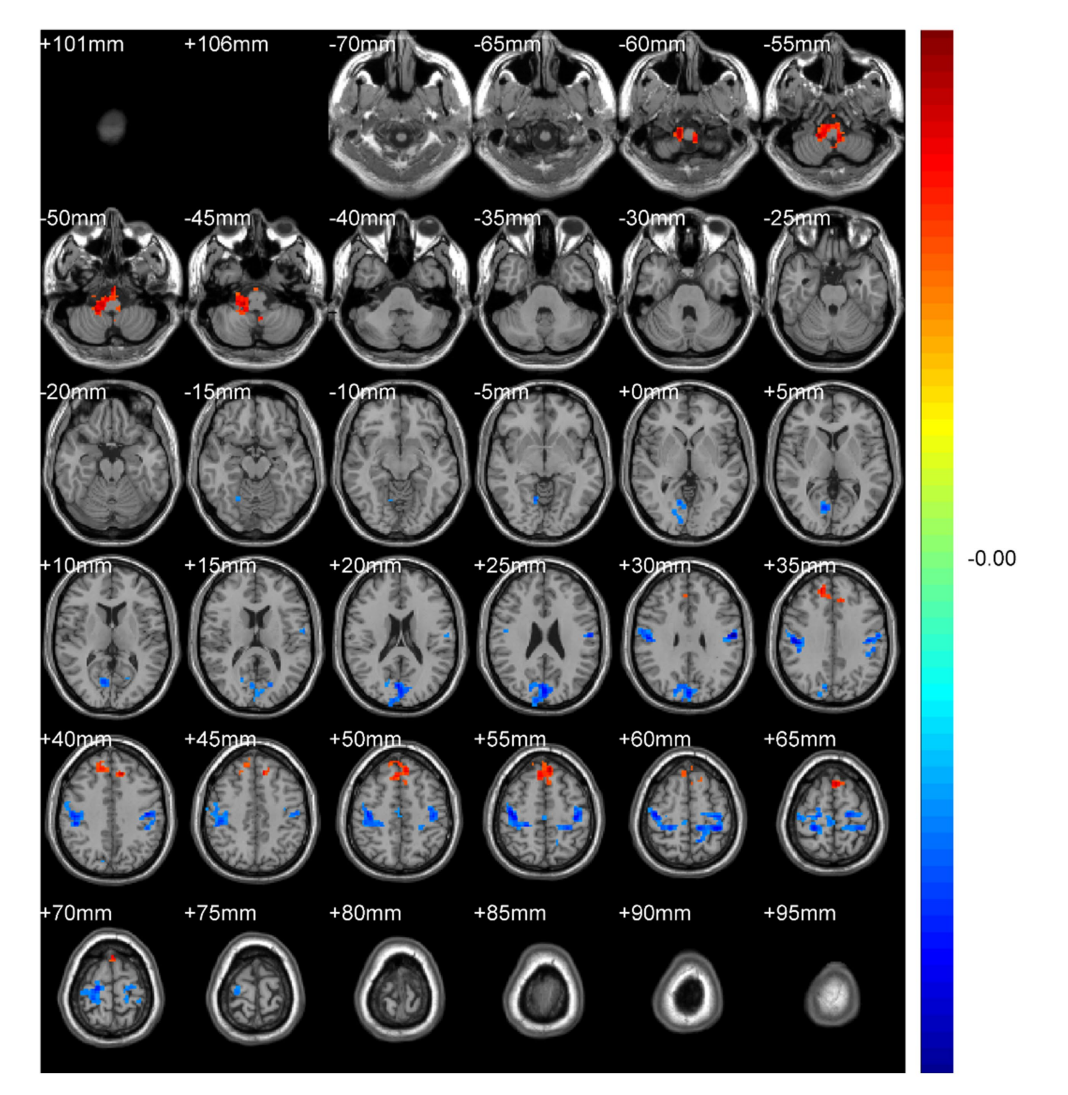


FIGURE 2

ZALFF analysis. Two-sample t-test results are presented. Areas in red indicate significantly increased zALFF value. Areas in blue indicate significantly decreased zALFF value. In the comparison of zALFF value between patient group compared to control group showed significantly increased zALFF in Cerebellum\_9\_R and right Frontal\_Sup\_Medial\_R.

TABLE 4 ReHo differences (SMKCC method).

Brain regions	Hemisphere	Cluster size	Cluster centroid MNI Coordinates			t-value
			Х	Υ	Z	
Postcentral	L	641	-57	-12	27	-5.2072
Postcentral	R	680	27	-21	75	-5.5139

-18, 54; cluster = 450; t = -5.0403), and right precuneus (MNI - 3, -45, 57; cluster = 110; t = -4.5909).

Degree centrality (DC) (Tables 9–12; Figures 8–11): Across DC variants, cerebellar Crus I/II showed increased degree centrality, whereas motor and orbitofrontal hubs showed decreased degree centrality.

Binary-SmDegreeCentrality: left Crus I (MNI 30, -75, -21; cluster = 1,724; t = 3.9172) showed increased degree centrality; right superior orbital frontal gyrus (MNI 21, 21, -27; cluster = 599;

t = -3.7685) and left precentral gyrus (MNI 15, -9, 69; cluster = 1,064; t = -4.7716) showed decreased degree centrality.

Binary-SzDegreeCentrality: left Crus I (MNI 30, -75, -24; cluster = 1,171; t = 4.2187) and right Angular gyrus (MNI 42, -54, 54; cluster = 781; t = 3.6977) showed increased degree centrality; right Putamen (MNI 21, 21, -27; cluster = 1,021; t = -3.9621), left inferior orbital frontal gyrus (MNI -21, 18, -24; cluster = 594; t = -3.8329) and left precentral gyrus (MNI 15, -9, 69; cluster = 1,277; t = -4.8323) showed decreased degree centrality.

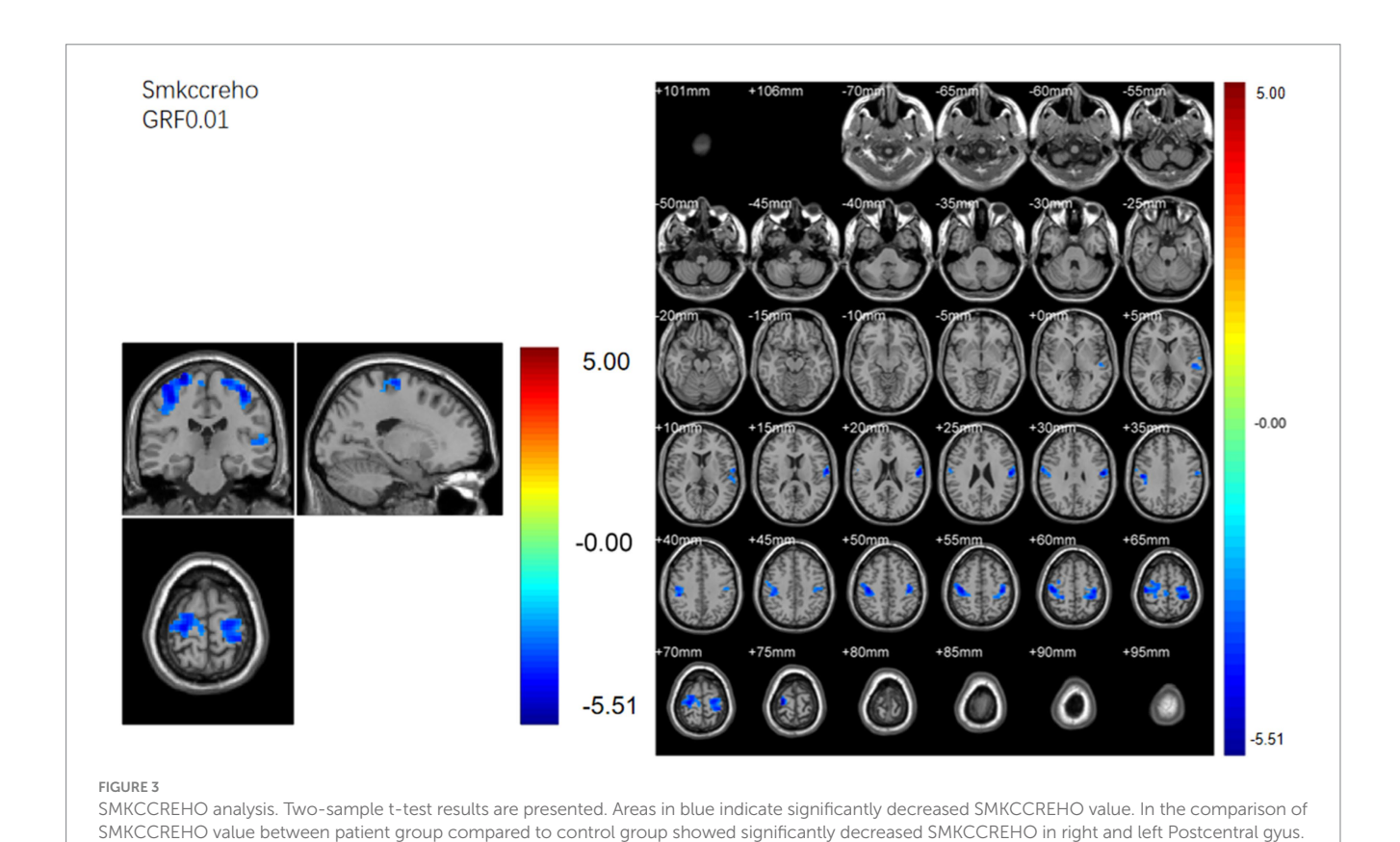


TABLE 5 Functional connection with the left postcentral gyrus as the seed point for patient group compared to subjects with control group.

Brain regions	Hemisphere	Cluster size	Cluster ce	t-value		
			Х	Y	Z	
Cerebelum_Crus1	L	131	-42	-63	-36	4.4727
Thalamus	L	67	-18	-21	12	4.1848
Precentral	R	104	39	-15	51	-4.1961
Postcentral	L	113	-27	-33	66	-4.1962
Paracentral_Lobule	R	160	9	-21	69	-4.3763

TABLE 6 Functional connection with the right Postcentral gyrus as the seed point for patient group compared to subjects with control group.

Brain regions	Hemisphere	Cluster size	Cluster cent	rdinates	t-value	
			Х	Υ	Z	
Cerebelum_Crus2	L	129	-30	-57	-45	4.4861
Cerebelum_Crus1	R	127	15	-51	-45	4.6384
Temporal_Sup	L	197	-54	-12	27	-5.1077
Calcarine	R	76	12	-51	0	-3.9785
Precentral	R	316	39	-15	54	-5.2055
Postcentral	L	137	-45	-15	54	-4.4583

Weighted-SmDegreeCentrality: left Crus I (MNI 30, -75, -24; cluster = 1,250; t = 3.8040) showed increased degree centrality; right superior orbital frontal gyrus (MNI 21, 21, -27; cluster = 690; t = -3.8201) and left precentral gyrus (MNI 18, -9, 69; cluster = 1,037; t = -4.6758) showed decreased degree centrality.

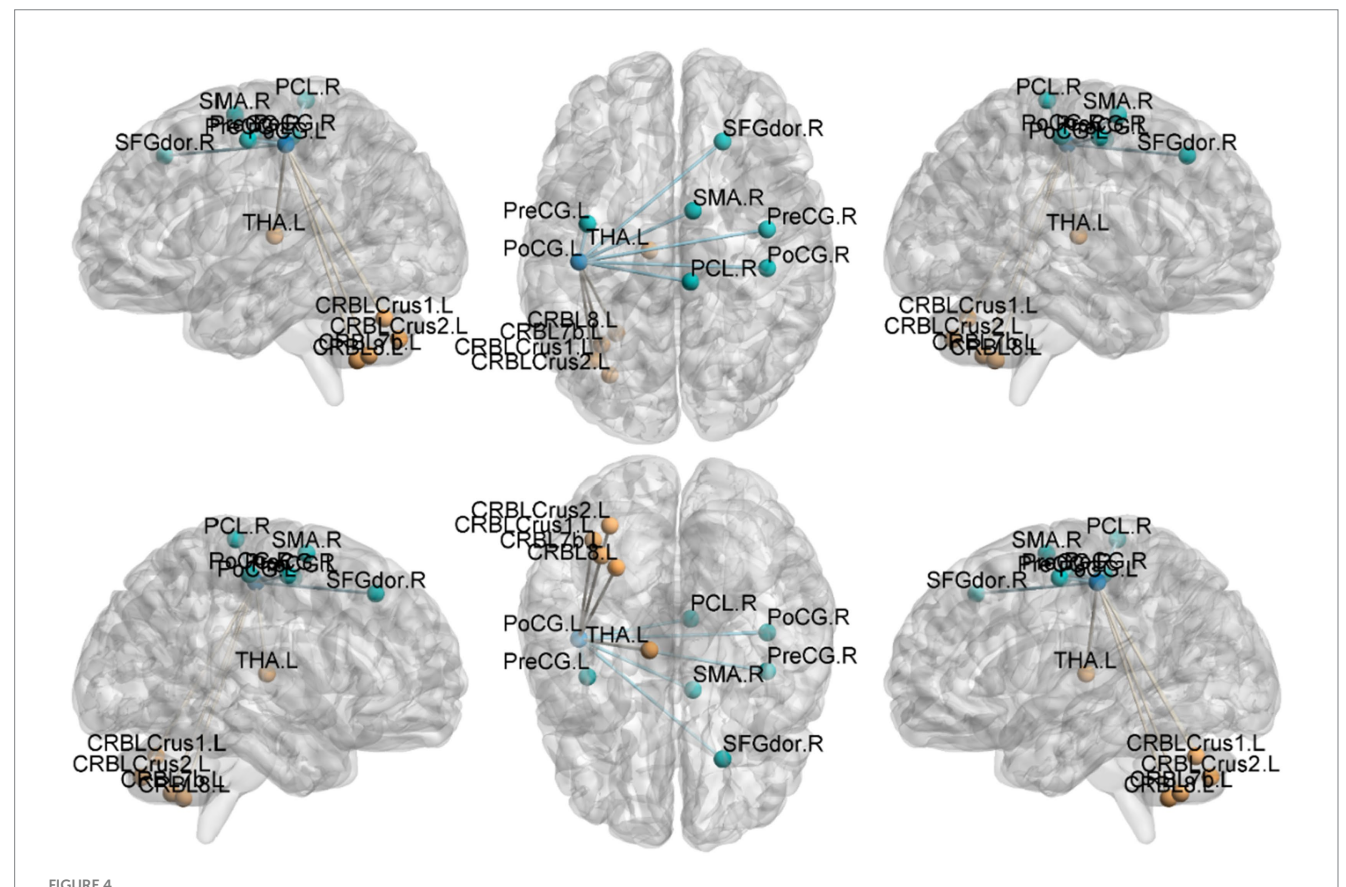
WeightedSzDegreeCentrality: left Crus I (MNI -6, -81, -18; cluster = 1,947; t = 4.1556) showed increased degree centrality; right superior orbital frontal gyrus (MNI 21, 21, -27; cluster = 732; t = -3.7573) and left precentral gyrus (MNI 18, -9, 69; cluster = 1,633; t = -4.7346) showed decreased degree centrality.

TABLE 7 Functional connection with the left precentral gyrus as the seed point for patient group compared to control group.

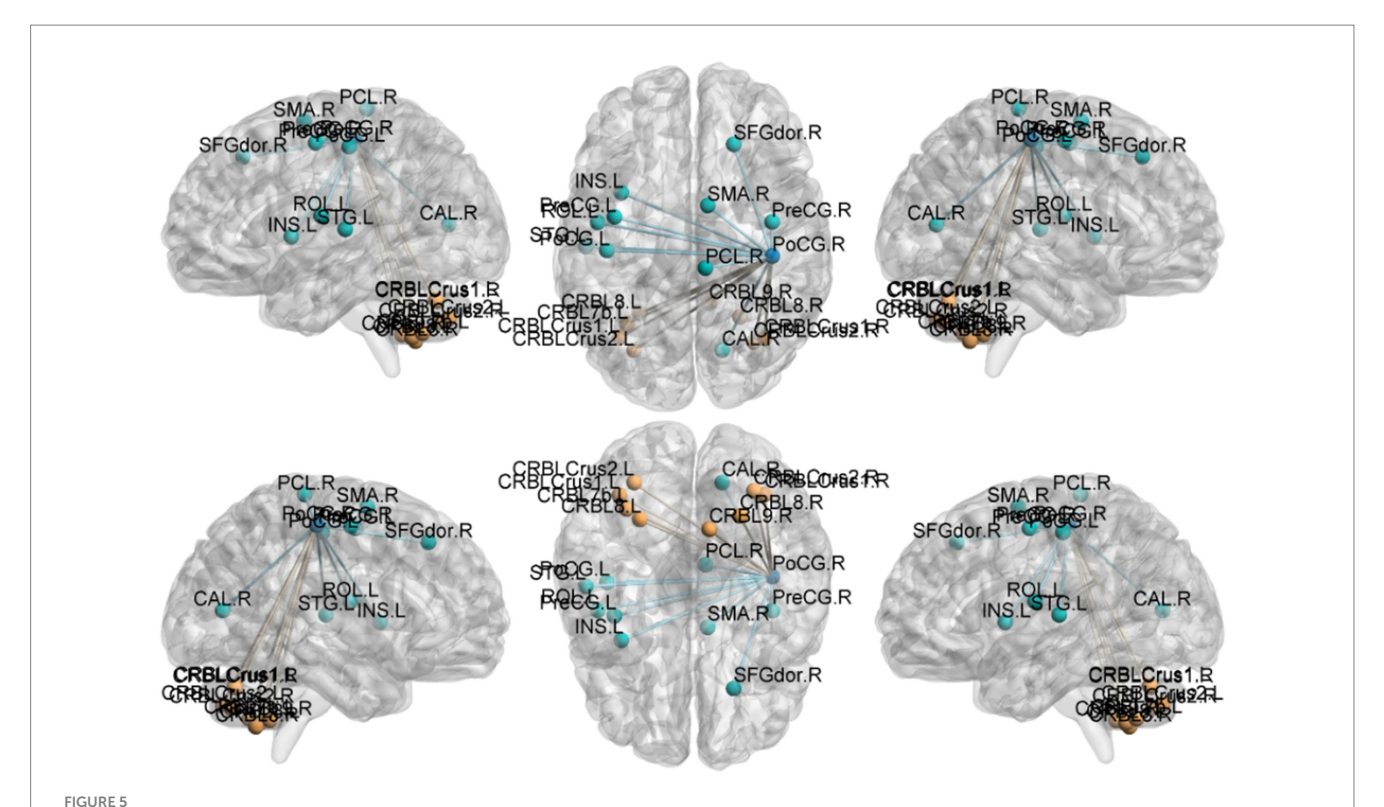
Brain regions	Hemisphere	Cluster size	Cluster ce	oordinates	t-value	
			Х	Y	Z	
Cerebelum_Crus2	L	198	-42	-60	-39	4.495
Temporal_Sup	L	115	-45	-18	12	-4.5627
Thalamus	R	58	15	-15	12	4.5659
Cuneus	L	63	-9	-84	24	-4.0804
Thalamus	L	55	-15	-21	12	4.9435
Postcentral	L	321	-39	-27	57	-4.7458
Postcentral	R	143	36	-36	60	-4.6398
Frontal_Sup	R	108	27	-24	75	-4.233

TABLE 8 Functional connection with the right precentral gyrus as the seed point for patient group compared to control group.

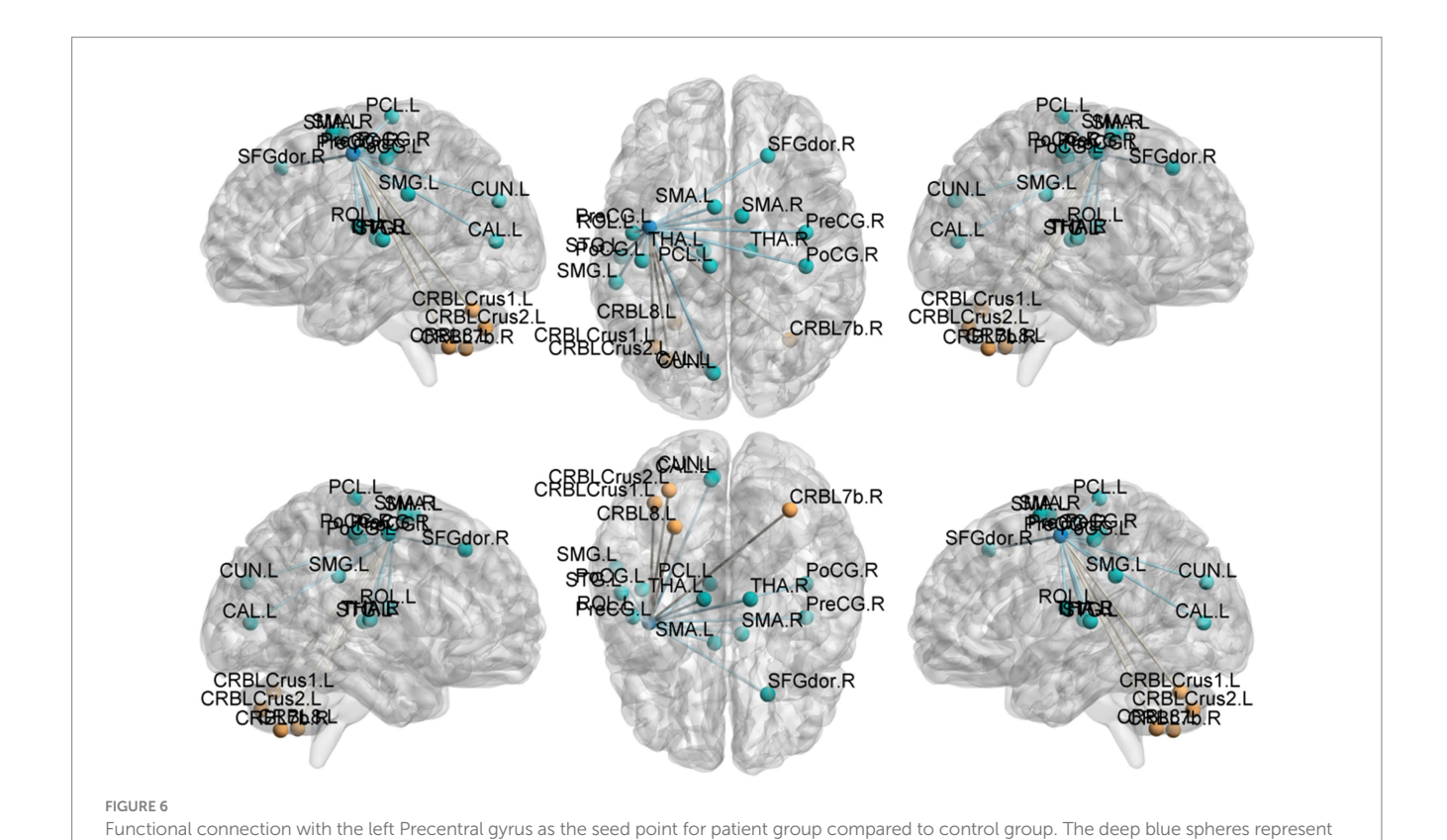
Brain regions	Hemisphere	Cluster size	uster size Cluster centroid MNI Coordinates				
			Х	Υ	Z		
Cerebelum_Crus1	R	235	30	-75	-36	5.0247	
Cerebelum_Crus2	L	214	-3	-69	-30	4.685	
Temporal_Sup	R	200	-45	-18	12	-5.1304	
Postcentral	L	186	-42	-18	51	-4.0706	
Postcentral	R	450	42	-18	54	-5.0403	
Precuneus	R	110	-3	-45	57	-4.5909	



Functional connection with the left Postcentral gyrus as the seed point for patient group compared to control group. The deep blue spheres represent regions of interest, the light blue spheres represent brain regions with decreased functional connectivity to the regions of interest, and the orange spheres represent brain regions with increased functional connectivity to the regions of interest.



Functional connection with the right Postcentral gyrus as the seed point for patient group compared to control group. The deep blue spheres represent regions of interest, the light blue spheres represent brain regions with decreased functional connectivity to the regions of interest, and the orange spheres represent brain regions with increased functional connectivity to the regions of interest.



regions of interest, the light blue spheres represent brain regions with decreased functional connectivity to the regions of interest, and the orange

spheres represent brain regions.

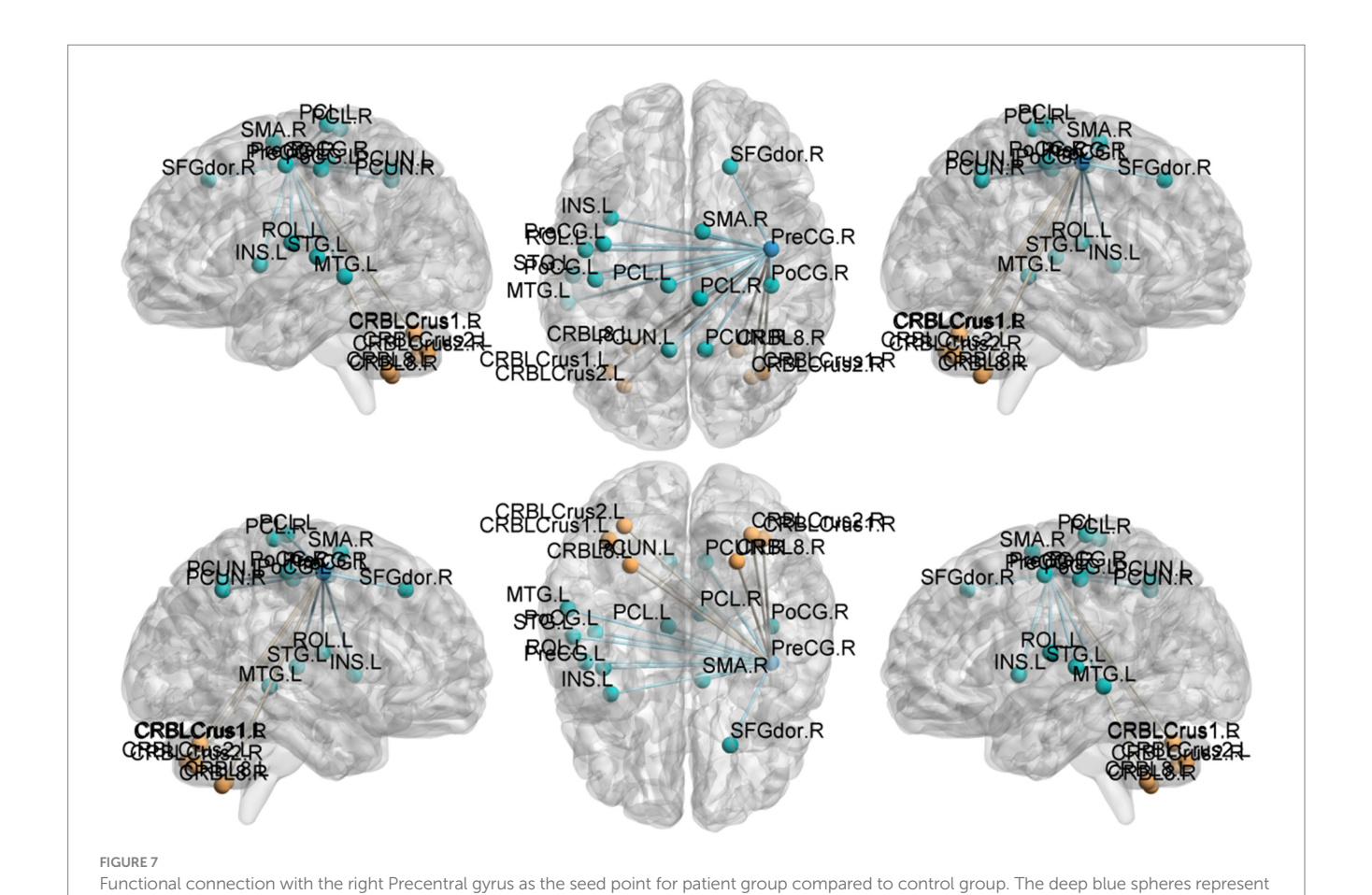


TABLE 9 DegreeCentrality (Bi-SmDegreeCentrality).

Brain regions	Hemisphere	Cluster size	Cluster ce	oordinates	t-value	
			Х	Y	Z	
Cerebelum_Crus1	L	1724	30	-75	-21	3.9172
Frontal_Sup_Orb	R	599	21	21	-27	-3.7685
Precentral	L	1,064	15	-9	69	-4.7716

regions of interest, the light blue spheres represent brain regions with decreased functional connectivity to the regions of interest, and the orange

spheres represent brain regions with increased functional connectivity to the regions of interest.

TABLE 10 DegreeCentrality (Bi-SzDegreeCentrality).

Brain regions	Hemisphere	Cluster size	Cluster ce	oordinates	t-value	
			Х	Y	Z	
Cerebelum_Crus1	L	1,171	30	-75	-24	4.2187
Putamen	R	1,021	21	21	-27	-3.9621
Frontal_Inf_Orb	L	594	-21	18	-24	-3.8329
Angular	R	781	42	-54	54	3.6977
Precentral	L	1,277	15	-9	69	-4.8323

# 4 Discussion

Across complementary resting-state metrics—regional activity (mALFF/zALFF), local synchrony (ReHo), pairwise coupling (seed-based FC), and graph metrics (degree centrality,

DC)—patients with spinal diseases–related pain exhibit a coherent reorganization of the sensorimotor–thalamo–cerebellar system. Convergent evidence indicates (i) down-regulation within S1/M1, reflected by lower ALFF/zALFF, reduced ReHo, diminished DC, and weaker intra-sensorimotor FC; and (ii) up-weighting of

 ${\sf TABLE~11~DegreeCentrality~(weighted-SmDegreeCentrality)}.$ 

Brain regions	Hemisphere	Cluster size	Cluster centroid MNI coordinates			t-value
			X	Y	Z	
Cerebelum_Crus1	L	1,250	30	-75	-24	3.804
Frontal_Sup_Orb	R	690	21	21	-27	-3.8201
Precentral	L	1,037	18	-9	69	-4.6758

TABLE 12 DegreeCentrality (weighted-SzDegreeCentrality).

Brain regions	Hemisphere	Cluster size	Cluster centroid MNI Coordinates			t-value
			Х	Y	Z	
Cerebelum_Crus1	L	1947	-6	-81	-18	4.1556
Frontal_Sup_Orb	R	732	21	21	-27	-3.7573
Precentral	L	1,633	18	-9	69	-4.7346

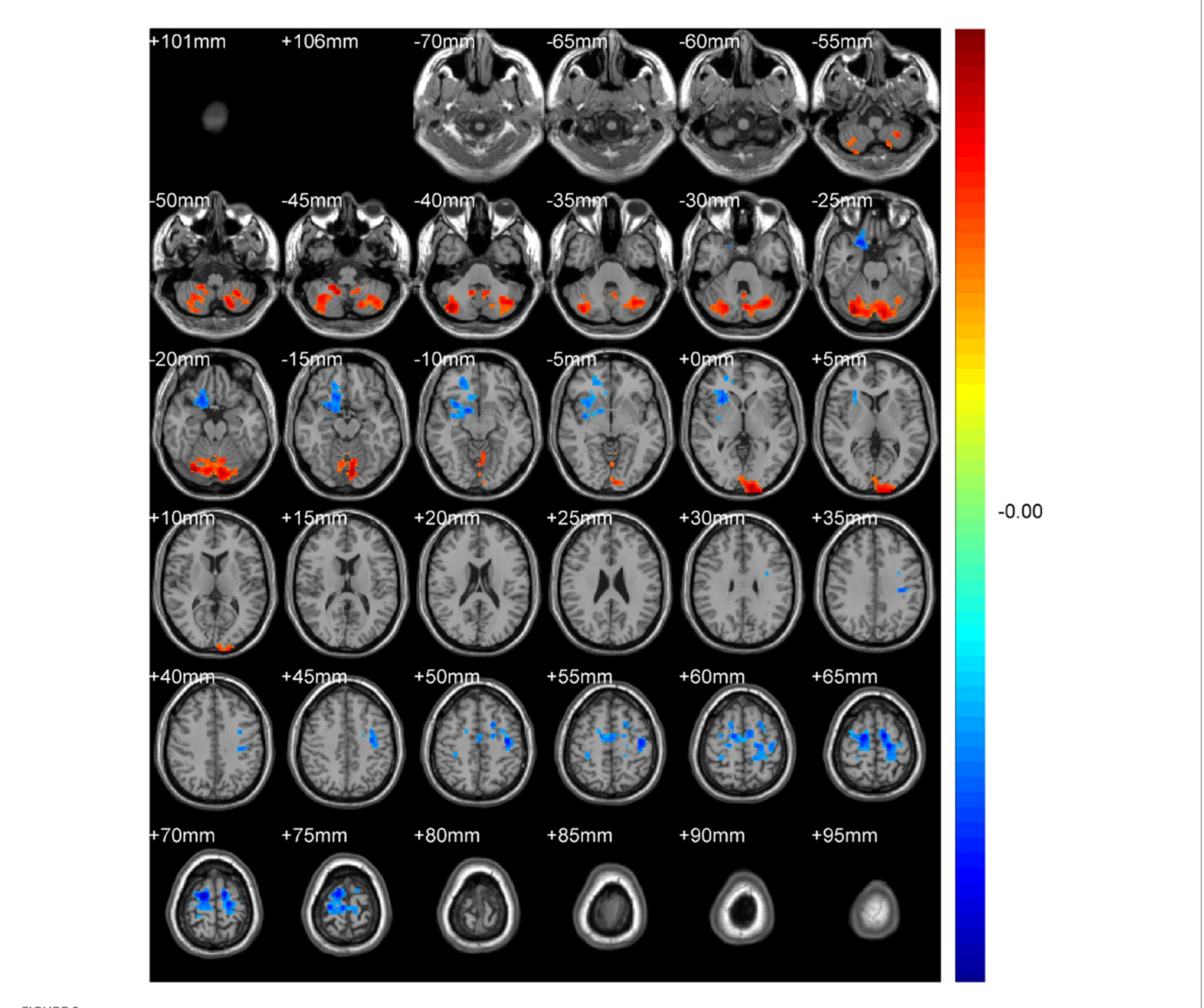


FIGURE 8
DegreeCentrality(Bi-SmDegreeCentrality). Areas in blue indicate significantly decreased value, areas in red indicate significantly increased value.

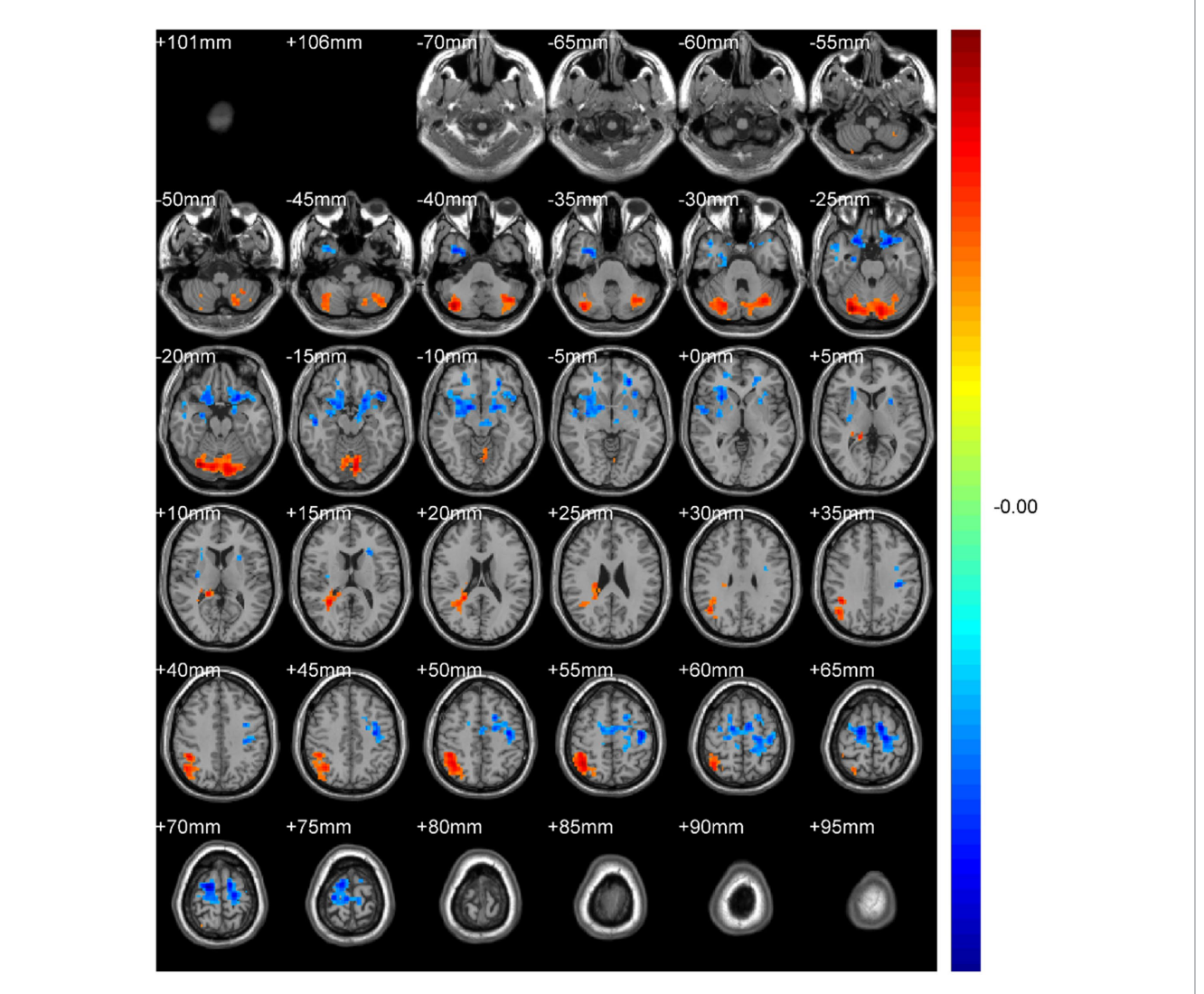


FIGURE 9

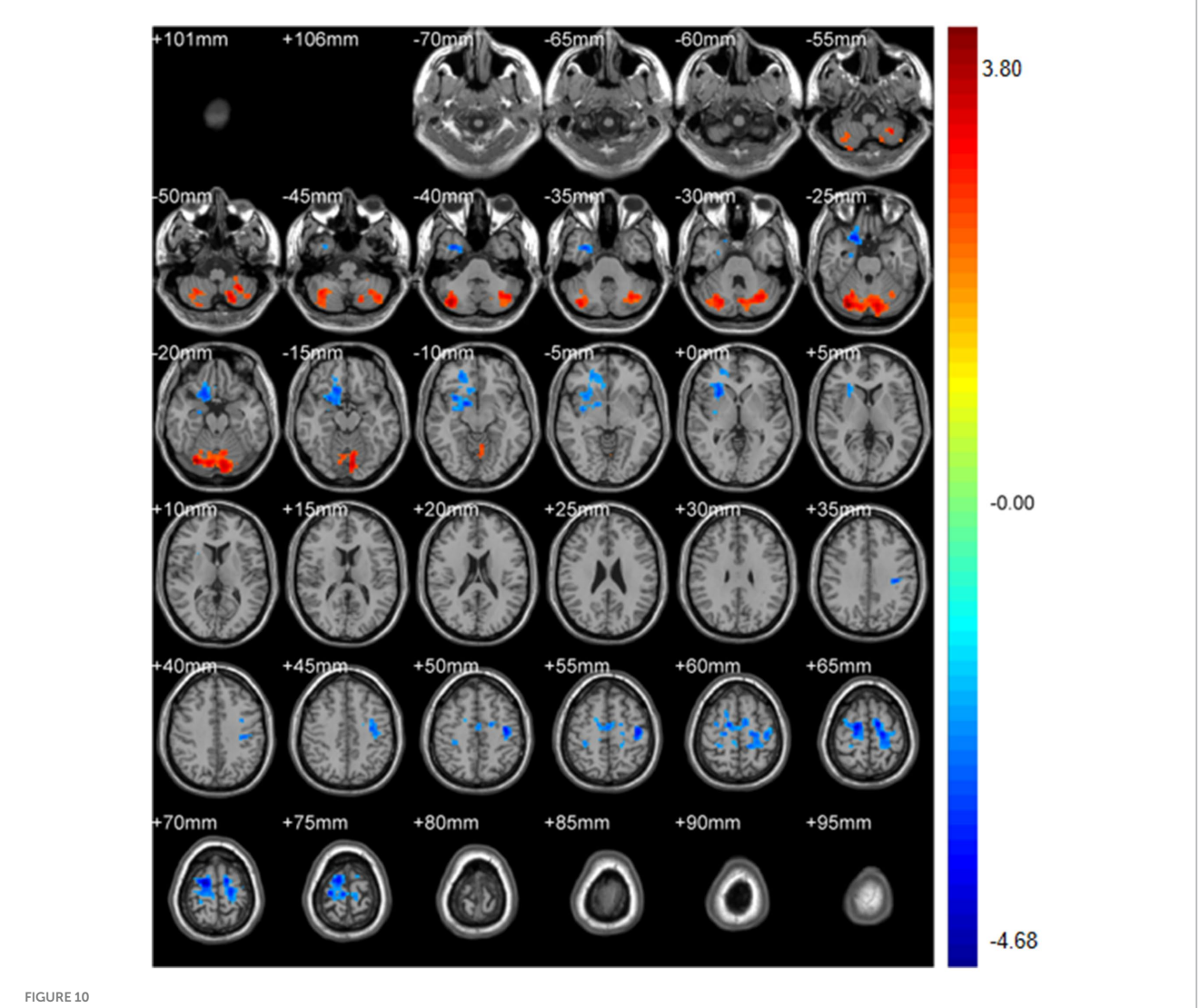
DegreeCentrality(Bi-SzDegreeCentrality). Areas in blue indicate significantly decreased value, areas in red indicate significantly increased value.

cerebellar nodes, including increased ALFF/zALFF in Cerebellum lobule IX and consistently elevated DC in Crus I/II across binary and weighted thresholds. Beyond the primary motor system, reduced coupling with superior temporal gyrus, calcarine/cuneus, and precuneus/DMN suggests broader consequences for auditory-temporal integration, early visual processing, and default-mode subsystems. Laterality was modest overall in the network-level synthesis, though the voxelwise analyses highlight pronounced right lobule IX hyperactivity (ALFF t = 4.84) and left Crus I hyperconnectivity (DC peak t = 4.22), nominating postcentral and cerebellar clusters as hubs in a shift from cortical sensorimotor dominance toward cerebellar–subcortical coordination.

The combined pattern is compatible with sensorimotor dysrhythmia and compensatory gating models in chronic pain. The dual-mode cerebellar signature suggests subregional dissociation: lobule IX may contribute to more direct nociceptive integration (34), whereas Crus I appears to participate in compensatory network reorganization via enhanced thalamocortical coupling (35). These observations align with literature on

cerebellar involvement in pain anticipation (36) and descending modulatory control (37). The prefrontal findings indicate functional segregation within medial PFC, with anterior (t = 4.28) versus posterior (t = 4.10) subregions showing differential activation that plausibly map onto the affective (38) and cognitive-evaluative (39) dimensions of pain, respectively, and thus motivate subregion-specific modulation strategies. Meanwhile, the preserved thalamic coupling (e.g., left thalamus t = 4.94) in the context of cortical hypoactivity is consistent with roles proposed for central sensitization (40) and enhanced nociceptive relay (41). Notably, age effects were negligible in these data, in keeping with reports of minimal association between age and clinical pain perception in similar cohorts (42, 43), suggesting the observed signatures are primarily symptom-related rather than age-driven.

Together, these results nominate cerebellar Crus I/II and sensorimotor–thalamic loops as testable targets for neuromodulation or rehabilitation. In particular, Crus I/II DC and cerebello–S1/M1 FC emerge as plausible network-level readouts for patient stratification and treatment monitoring. The



DegreeCentrality(weighted-SmDegreeCentrality). Areas in blue indicate significantly decreased value, areas in red indicate significantly increased value.

observed prefrontal subspecialization further implies subregionspecific stimulation or neurofeedback protocols tailored to affective versus cognitive pain components.

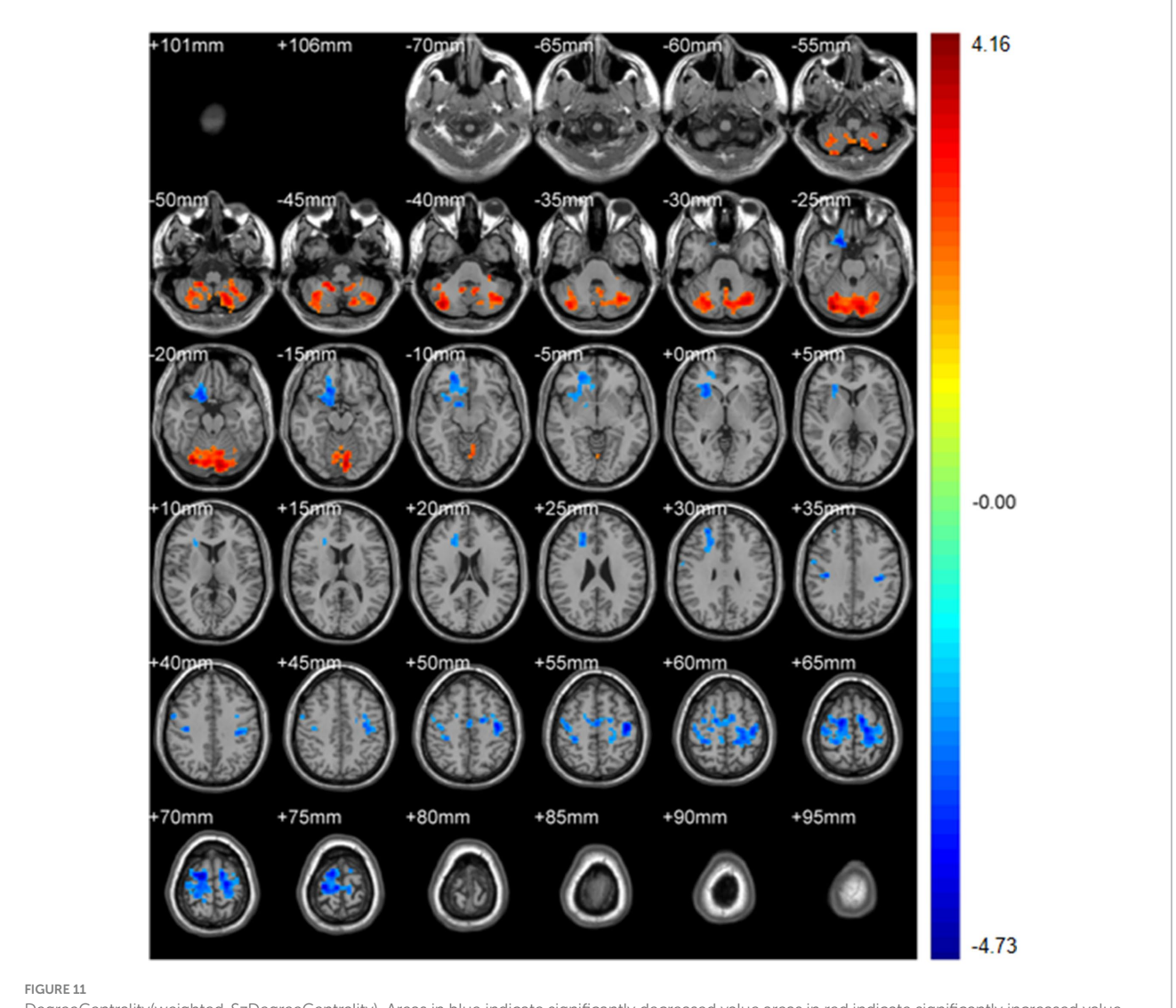
Limitations: This work is retrospective with a modest sample size, limiting causal inference and external generalizability. Clinical heterogeneity (spinal pathology, medication, pain duration/treatment history) may introduce variance beyond modeled covariates. Results are group-level and not individually predictive. Graph metrics such as DC can be sensitive to thresholding and pipeline parameters; although convergence across binary and weighted thresholds increases confidence, absolute DC values warrant cautious interpretation. Despite stringent motion controls, residual micromovements and state factors (attention, medication) cannot be fully excluded. Finally, the absence of behavioral correlations (sensorimotor performance, detailed pain phenotyping) constrains mechanistic claims.

Future directions: Prospective, phenotype-stratified and longitudinal cohorts with harmonized acquisition and open, standardized pipelines should test the stability, specificity, and prognostic value of these signatures. Interventional designs

(neuromodulation, neurofeedback, targeted rehabilitation) can probe causality by tracking Crus I/II DC and cerebellosensorimotor FC as mechanistic endpoints alongside clinical outcomes. Multimodal integration (structural, diffusion, and task paradigms) and behavioral anchoring will be essential to refine theranostic utility.

# 5 Conclusion

Patients with spinal diseases-related pain show a reproducible, multimodal reconfiguration of resting-state networks: down-regulation of primary sensorimotor cortices and up-weighting of cerebellar nodes (lobule IX, Crus I/II), with strengthened cerebello-sensorimotor and thalamo-cortical coupling and reduced interactions with temporal, occipital, and precuneus/DMN regions. Prefrontal subspecialization further suggests altered evaluative-affective control. While associative, this coherent signature refines the central phenotype as a shift of network load toward cerebellar-subcortical loops and nominates



DegreeCentrality(weighted-SzDegreeCentrality). Areas in blue indicate significantly decreased value, areas in red indicate significantly increased value.

cerebellar (Crus I/II, lobule IX), thalamic, and S1/M1 circuits as testable targets. Network-level readouts—particularly Crus I/II degree centrality and cerebello–S1/M1 connectivity—warrant prospective evaluation as biomarkers for stratification and treatment monitoring.

# Data availability statement

The raw data supporting the conclusions of this article will be made available by the authors, without undue reservation.

# **Ethics statement**

The studies involving humans were approved by Ethical Approval Number: 20240902113233506. The studies were conducted in accordance with the local legislation and institutional requirements. The participants provided their written informed consent to

participate in this study. Written informed consent was obtained from the individual(s) for the publication of any potentially identifiable images or data included in this article.

# **Author contributions**

JZ: Data curation, Writing – review & editing. NW: Supervision, Writing – review & editing. L-MR: Investigation, Writing – review & editing. XS: Data curation, Validation, Writing – original draft. J-PZ: Data curation, Formal analysis, Writing – review & editing. YZ: Investigation, Methodology, Project administration, Writing – review & editing.

# **Funding**

The author(s) declare that no financial support was received for the research and/or publication of this article.

# Conflict of interest

The authors declare that the research was conducted in the absence of any commercial or financial relationships that could be construed as a potential conflict of interest.

# Generative AI statement

The authors declare that no Gen AI was used in the creation of this manuscript.

Any alternative text (alt text) provided alongside figures in this article has been generated by Frontiers with the support of artificial

intelligence and reasonable efforts have been made to ensure accuracy, including review by the authors wherever possible. If you identify any issues, please contact us.

# Publisher's note

All claims expressed in this article are solely those of the authors and do not necessarily represent those of their affiliated organizations, or those of the publisher, the editors and the reviewers. Any product that may be evaluated in this article, or claim that may be made by its manufacturer, is not guaranteed or endorsed by the publisher.

# References

- GBD 2017 Disease and Injury Incidence and Prevalence Collaborators. Global, regional, and national incidence, prevalence, and years lived with disability for 354 diseases and injuries for 195 countries and territories, 1990–2017: a systematic analysis for the global burden of disease study 2017. *Lancet*. (2018) 392:1789–858. doi: 10.1016/S0140-6736(18)32279-7
- 2. Webers C, Grimm S, van Tubergen A, van Gaalen F, van der Heijde D, Joore M, et al. The value of correctly diagnosing axial spondyloarthritis for patients and society. *Semin Arthritis Rheum.* (2023) 62:152242. doi: 10.1016/j.semarthrit.2023.152242
- 3. van Gaalen FA, Rudwaleit M. Challenges in the diagnosis of axial spondyloarthritis. Best Pract Res Clin Rheumatol. (2023) 37:101871. doi: 10.1016/j.berh.2023.101871
- 4. Knezevic NN, Candido KD, Vlaeyen JWS, Van Zundert J, Cohen SP. Low back pain. Lancet. (2021) 398:78–92. doi: 10.1016/S0140-6736(21)00733-9
- 5. Mayoral Rojals V, Canós Verdecho Á, Soler López BThe Team Duo. Assessment of the management of patients with chronic pain referred to a specialized pain unit: a cross-sectional multicenter study (the DUO project). *J Clin Med.* (2022) 11:3586. doi: 10.3390/jcm11133586
- 6. Attal N, Bouhassira D, Colvin L. Advances and challenges in neuropathic pain: a narrative review and future directions.  $Br\ J\ Anaesth$ . (2023) 131:79–92. doi: 10.1016/j.bja.2023.04.021
- 7. Kirnaz S, Capadona C, Lintz M, Kim B, Yerden R, Goldberg JL, et al. Pathomechanism and biomechanics of degenerative disc disease: features of healthy and degenerated discs. *Int J Spine Surg.* (2021) 15:10–25. doi: 10.14444/8052
- 8. Tang SN, Walter BA, Heimann MK, Gantt CC, Khan SN, Kokiko-Cochran ON, et al. In vivo mouse intervertebral disc degeneration models and their utility as translational models of clinical discogenic back pain: a comparative review. *Front Pain Res.* (2022) 3:894651. doi: 10.3389/fpain.2022.894651
- 9. Yan J, Wu LG, Zhang M, Fang T, Pan W, Zhao JL, et al. miR-328-5p induces human intervertebral disc degeneration by targeting WWP2. *Oxidative Med Cell Longev*. (2022) 2022:3511967. doi: 10.1155/2022/3511967
- 10. Baliki MN, Petre B, Torbey S, Herrmann KM, Huang L, Schnitzer TJ, et al. Corticostriatal functional connectivity predicts transition to chronic back pain. *Nat Neurosci.* (2012) 15:1117–9. doi: 10.1038/nn.3153
- 11. Hashmi JA, Baliki MN, Huang L, Baria AT, Torbey S, Hermann KM, et al. Shape shifting pain: chronification of back pain shifts brain representation from nociceptive to emotional circuits. *Brain*. (2013) 136:2751–68. doi: 10.1093/brain/awt211
- 12. Seminowicz DA, Wideman TH, Naso L, Hatami-Khoroushahi Z, Fallatah S, Ware MA, et al. Effective treatment of chronic low back pain in humans reverses abnormal brain anatomy and function. *J Neurosci*. (2011) 31:7540–50. doi: 10.1523/JNEUROSCI.5280-10.2011
- $13.\,Menon\,V.$  20 years of the default mode network: a review and synthesis. Neuron. (2023) 111:2469-87. doi: 10.1016/j.neuron.2023.04.023
- 14. Kong J, Spaeth RB, Wey HY, Cheetham A, Cook AH, Jensen K, et al. S1 is associated with chronic low back pain: a functional and structural MRI study. *Mol Pain.* (2013) 9:43. doi: 10.1186/1744-8069-9-43
- 15. Worsley KJ, Liao CH, Aston J, Petre V, Duncan GH, Morales F, et al. A general statistical analysis for fMRI data. *NeuroImage*. (2002) 15:1–15. doi: 10.1006/nimg.2001.0933
- 16. Calhoun VD, Adali T, Pearlson GD, Pekar JJ. A method for making group inferences from functional MRI data using independent component analysis. *Hum Brain Mapp*. (2001) 14:140–51. doi: 10.1002/hbm.1048
- 17. Loggia ML, Chonde DB, Akeju O, Arabasz G, Catana C, Edwards RR, et al. Evidence for brain glial activation in chronic pain patients. *Brain*. (2015) 138:604–15. doi: 10.1093/brain/awu377

- 18. Uğurbil K. Development of functional imaging in the human brain (fMRI); the University of Minnesota experience. *NeuroImage*. (2012) 62:613–9. doi: 10.1016/j.neuroimage.2012.01.135
- 19. Wang C, Pan Y, Zhang W, Zhao H, Liu S, Xu Y, et al. Positive regulatory domain I-binding factor 1 mediates peripheral nerve injury-induced nociception in mice by repressing Kv4.3 channel expression. *Anesthesiology*. (2021) 134:435–56. doi: 10.1097/ALN.0000000000003654
- 20. Edison P. Brain connectivity: a journal of clinical neurology, neuroscience, & neuroimaging advancing the field of neurology. *Brain Connect.* (2022) 12:847–9. doi: 10.1089/brain.2022.29043.editorial
- 21. Wang Y, Weng XC. Progress in functional neuroimaging studies of human skill learning. Adv Psychol Sci. (2003) 11:136–40.
- 22. Buchbinder BR. Functional magnetic resonance imaging In: MJ Aminoff, F Boller and DF Swaab, editors. Handbook of clinical neurology, vol. *135*. Amsterdam: Elsevier (2016), 61–92.
- 23. Zhang Y, Mao Z, Pan L, Ling Z, Liu X, Zhang J, et al. Frequency-specific alterations in cortical rhythms and functional connectivity in trigeminal neuralgia. Brain Imaging Behav. (2019) 13:1497–509. doi: 10.1007/s11682-019-00105-8
- 24. Fu Z, Hu N, Pan CH, Zhang J, Wang XQ, Wang TH, et al. Advance of functional magnetic resonance imaging in motor function of hand in patients with stroke. *Chin J Rehabil Theory Pract.* (2015) 21:1277–81.
- 25. Friston KJ, Holmes AP, Poline JB, Grasby PJ, Williams SC, Frackowiak RS, et al. Analysis of fMRI time-series revisited. *NeuroImage.* (1995) 2:45–53. doi: 10.1006/nimg.1995.1007
- 26. Solomon P, Davydov DM. Chronic pain and the brain impairment: introducing a translational neuroscience-based metric. *Pain Med.* (2016) 17:799–802. doi: 10.1093/pm/pnw024
- 27. Zou QH, Zhu CZ, Yang Y, Zuo XN, Long XY, Cao QJ, et al. An improved approach to detection of amplitude of low-frequency fluctuation (ALFF) for resting-state fMRI: fractional ALFF. J Neurosci Methods. (2008) 172:137–41. doi: 10.1016/j.jneumeth. 2008.04.012
- 28. Zhao G, Zhan Y, Zha J, Cao Y, Zhou F, He L. Abnormal intrinsic brain functional network dynamics in patients with cervical spondylotic myelopathy. *Cogn Neurodyn*. (2023) 17:1201–11. doi: 10.1007/s11571-022-09807-0
- 29. Jia XZ, Wang J, Sun HY, Zhang H, Liao W, Wang Z, et al. RESTplus: an improved toolkit for resting-state functional magnetic resonance imaging data processing. *Sci Bull.* (2019) 64:953–4. doi: 10.1016/j.scib.2019.05.008
- 30. Jia XZ, Sun JW, Ji GJ, Liao W, Lv YT, Wang J, et al. Percent amplitude of fluctuation: a simple measure for resting-state fMRI signal at single voxel level. *PLoS One.* (2020) 15:e0227021. doi: 10.1371/journal.pone.0227021
- 31. Zang Y, Jiang T, Lu Y, He Y, Tian L. Regional homogeneity approach to fMRI data analysis. *NeuroImage*. (2004) 22:394–401. doi: 10.1016/j.neuroimage.2003.12.030
- 32. Wu G, Liao W, Stramaglia S, Ding J, Chen H, Marinazzo D. A blind deconvolution approach to recover effective connectivity brain networks from resting-state fMRI data. *Med Image Anal.* (2013) 17:365–74. doi: 10.1016/j.media.2013.01.003
- 33. Penny WD, Friston KJ, Ashburner J, Kiebel S, Nichols TE. Statistical parametric mapping: The analysis of functional brain images. Amsterdam: Academic Press (2007).
- 34. Tedesco AM, Chiricozzi FR, Clausi S, Lupo M, Molinari M, Leggio MG. The cerebellar cognitive profile. *Brain*. (2011) 134:3672–86. doi: 10.1093/brain/awr266
- 35. Dong F, Yu L, Lin F, Feng P, Wang C, Zhang Y, et al. An atlas of neuropathic pain-associated molecular pathological characteristics in the mouse spinal cord. *Commun Biol.* (2025) 8:70. doi: 10.1038/s42003-025-07506-0

- 36. Stoodley CJ, Schmahmann JD. Functional topography in the human cerebellum: a meta-analysis of neuroimaging studies. *NeuroImage*. (2009) 44:489–501. doi: 10.1016/j.neuroimage.2008.08.039
- 37. Noseda R, Schain AJ, Borsook D. Cerebro-cerebellar networks in migraine symptoms and headache. *Front Pain Res (Lausanne)*. (2022) 3:1002147. doi: 10.3389/fpain.2022.940923
- 38. Wiech K, Kalisch R, Weiskopf N, Pleger B, Stephan KE, Dolan RJ. Anterolateral prefrontal cortex mediates the analgesic effect of expected and perceived control over pain. *J Neurosci.* (2006) 26:11501–9. doi: 10.1523/JNEUROSCI.2568-06.2006
- 39. Wiech K, Tracey I. The influence of negative emotions on pain: behavioral effects and neural mechanisms. *NeuroImage*. (2009) 47:987–94. doi: 10.1016/j.neuroimage.2009. 05.059
- 40. Clarke S, Rogers R, Wanigasekera V, Fardo F, Pia H, Nochi Z, et al. Systematic review and coordinate-based meta-analysis to summarize the utilization of functional brain imaging in conjunction with human models of peripheral and central sensitization. *Eur J Pain.* (2024) 28:1069–94. doi: 10.1002/ejp.2251
- 41. Silemek AC, Chen H, Sati P, Gao W. The brain's first "traffic map" through unified structural and functional connectivity (USFC) modeling. *Commun Biol.* (2024) 7:1477. doi: 10.1038/s42003-024-07160-y
- 42. Zhou C, Wang C, Tian F, Liu X, Li H, Liu S, et al. The incidence of cervical spondylosis decreases with aging in the elderly, and increases with aging in the young and adult population: a hospital-based clinical analysis. *Clin Interv Aging.* (2016) 11:47–53. doi: 10.2147/CIA.S93118
- 43. Stueckle CA, Talarczyk S, Stueckle KF, Beisenherz C, Haage P. Rückenschmerz: ein Phänomen des Alters? Z Gerontol Geriatr. (2022) 55:489–95. doi: 10.1007/s00391-021-01912-9